RSC Advances




ROYAL SOCIETY OF CHEMISTRY

www.rsc.org/advances

RSC Advances

RSCPublishing

ARTICLE

# Synthesis and characterization of Pd-Ni core-shell nanocatalysts for alkaline glucose electrooxidation

Cite this: DOI: 10.1039/x0xx00000x

DOI: 10.1039/x0xx00000x

www.rsc.org/

Cheng-Chuan Chen, and Lin-Chi Chen*

$Pd_{shell}Ni_{core}$ catalysts decorated carboxylated multi-walled carbon nanotubes (Pd-Ni/C) are synthesized by a two-stage polyol method. The nano-sized Pd-Ni/C catalysts have a metal particle size range from 4.7 to 6.6 nm, $Pd_{shell}Ni_{core}$ nanoparticles, with the improved electrocatalytic activity and durability for electrocatalytic glucose oxidation reaction (GOR). X-ray diffraction (XRD), high resolution transmission electron microscopy (HR-TEM), scanning transmission electron microscope (STEM) and scanning electron microscopy with energy-dispersive X-ray spectroscopy (SEM-EDS) are used to characterize the crystalline structure, particle formation, crystalline nature and elemental distribution, respectively. Cyclic voltammetry (CV), Tafel analysis, chronoamperomtry (CA) and multi-cycle cyclic voltammetry (mCV) are determined for the electrochemical properties of the Pd-Ni/C catalysts. The results indicate that Pd-Ni/C (1:0.06) exhibits the highest ECSA of 78.0 $m^2$ $g^{-1}$ which is 4.5 times higher than that of Pd/C and as well as has a 1.5-fold higher GOR current density of 21.2 mA $cm^{-2}$. The stability of Pd-Ni/C catalyzed glucose is also significantly enhanced according to the results of the poisoning rate study and 200 cycling CV test. The highest Pd-Ni/C (1:0.06) catalyzed GOR current density of 34.2 mA $cm^{-2}$ is attained in 0.5 M glucose and 1.0 M NaOH alkaline medium.

## Introduction

Direct glucose fuel cell (DGFC) is one of the promising alternative power sources in the future because glucose, a six carbon sugar, is renewable, abundant and non-toxic in nature. The theoretical energy density of the complete glucose oxidation reaction (GOR) is 2870 kJ $mol^{-1}$ and the catalytic process can generate up to 24 electrons for one molecule of glucose.[1-3] DGFCs with the high power output have been developed by utilizing noble metal as catalysts and are intended to power electronic devices.[4-6] In the recent yeas, the extensive investigation of noble metal catalyzes GOR has been made to generate a higher electricity. It is reported that Platinum (Pt) based catalysts are widely used in DGFCs due to their high glucose catalytic activities.[7-10] However, the main obstacles to enhancing GOR performances on Pt-based catalysts are the high cost, low anti-poisoning ability and poor long-term durability. For this reason, there are many studies focusing on finding an idea catalyst to improve the GOR performance.[5, 11-13] Therefore, an alternative approach to developing non-Pt catalyst with the high catalytic activity has been wildly investigated.

Recently, Palladium (Pd) has been studied on methanol and glucose oxidation in alkaline medium and provides the effective improvement of electrocatalytic performances.[12, 14, 15] However, the catalytic activity of Pd monometallic catalyst is still not sufficient to reach a notably higher GOR current density. It has been known that Pd-based bimetallic catalysts can significantly enhance the activities in alkaline glucose electrooxidation including palladium-gold (Pd-Au) and palladium-rhodium (Pd-Rh).[4, 12] The improvement of glucose catalytic performance is ascribed to the increase of specific active surface sites, bifunctional mechanism and electronic effect. In this regard, Pd-based bimetallic catalysts are emerging as potential non-Pt catalysts for alkaline GOR.

Moreover, the cost of Pd is also a critical hurdle to use Pd-based catalysts in the commercial application. Hence, many researchers have paid more attention to developing Pd-based core-shell catalysts for lowering Pd loading.[16-18] The core-shell structure is one of the promising ways to reduce the cost of metal catalysts by replacing the core metal with other cheaper materials. In addition, the electrocatalytic activity and stability of the shell metal can be improved through the synergistic effect with the core metal.[16] It has been reported that a great deal of studies have been focused on finding a lower cost metal material as core metal (e.g., nickel, cobalt and silver, etc.).[16, 18, 19] Among of the commonly used core metals, Nickle (Ni) shows a remarkable improvement of catalytic performance on small organic molecules.[20] Therefore, Ni would be an idea candidate for the core metal in Pd-based core-shell electrocatalysts. The prepared catalysts with Pd as shell and the low-cost Ni as core are synthesized by the facile process with a two-stage polyol method.

It also has been known that carbon nanosupport is important for decorating nanosized metallic particles with the high catalyst dispersion. In this respect, carbon nanotube (CNT) is known as a promising carbon support because of its high specific surface area, electronic conductivity, chemical stability and interaction with metal catalysts.[14, 21, 22] Recently, it has been demonstrated that the functionalized multi-walled carbon nanotube (MWCNT) can provide sufficient binding sites and improve the dispersion of decorated

metal nanoparticles. According to our earlier study, carboxylated multi-walled carbon nanotube (cMWCNT) has a more appropriate surface property for the well dispersion of Pd nanoparticles. [14] In this work, cMWCNT is chosen as a carbon support material for $Pd_{shell}Ni_{core}$ catalysts in alkaline GOR investigation.

The Pd-Ni/C catalysts with a core-shell structure are synthesized using a two-stage polyol method and the synthesis method is illustrated in Fig. 1. [23] To the best of our knowledge, this is the first study to use a carbon supported $Pd_{shell}Ni_{core}$ anode catalyst for alkaline glucose electrooxidation. The physicochemical properties of the Pd-Ni/C catalysts with different precursor ratios of Pd to Ni are characterized by XRD, HR-TEM, STEM and SEM-EDS. The electrocatalytic performances of the ECSA, GOR current density, Tafel plot, pensioning rate, long-term cycling stability, activation energy and concentration effect are studied by CV and CA methods through the alkaline GOR. Finally, the optimal operation condition for Pd-Ni/C (1:0.06) is determined in this study.

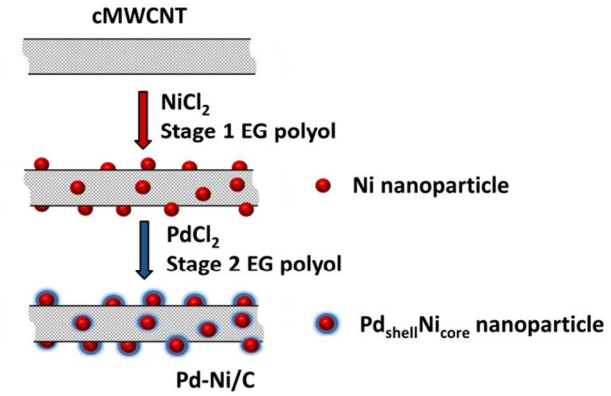


**Figure 1**. Illustration for a two-stage polyol synthesis method of the Pd-Ni/C core-shell catalyst.

## Experimental

### Materials and chemicals

All chemicals used are analytical grade without any further purification. Palladium chloride dihydrate ($PdCl_2 \cdot 2H_2O$) and nickel chloride hexahydrate ($NiCl_2 \cdot 6H_2O$) were used as the precursors. Ethylene glycol (EG) was used as the reducing agent and stabilizer for the two-stage polyol method. Sodium hydroxide (NaOH) and D-glucose were respectively used as the electrolyte and the fuel in the electrochemical investigation. All of the chemicals were purchased from Sigma-Aldrich. The conventional carboxylated MWCNT (carboxylation degree ca. 5%) was used as a metal catalyst carbon support and purchased from a local company (Golden Innovation, Taipei, Taiwan). Five percent Nafion® dispersion DE-520 (DuPont, Wilmington, Delaware, USA) was used to prepare the catalyst suspension. All aqueous solutions were prepared using double distilled water (18.2 MΩ cm).

### Synthesis of the Pd-Ni/C core-shell catalysts by a two-stage polyol method

cMWCNT supported $Pd_{shell}Ni_{core}$ catalysts Pd-Ni/C (1:x) with different precursor weight ratios of Pd to Ni (x=0.33, 0.14, 0.06, 0.03 and 0.02) were prepared by a two-stage polyol method as follows: The Ni/C dispersion was prepared by adding 100.0 mg of cMWCNT and the corresponding $NiCl_2 \cdot 6H_2O$ in 50 mL EG solution. When the homogeneous mixture was obtained, the pH of the mixture was adjusted to 11 by drop-wise addition of 0.5 mol $L^{-1}$ NaOH in EG. The prepared Ni precursor and cMWNCT mixture was cured at 140 $^oC$ with a gentle stirring for 2 h and then cooled to room temperature to form cMWCNT supported $Ni_{core}$ nanoparticles (Ni/C). For the preparation of $Pd_{shell}$ coated $Ni_{core}$ catalysts, the corresponding $PdCl_2 \cdot 2H_2O$ was mixed with the Ni/C under a gently stirring for 30 min. The prepared mixture was cured at 140 $^oC$ with a gentle stirring for 2 h and then cooled to room temperature to form cMWCNT supported $Pd_{shell}Ni_{core}$ nanoparticles (Pd-Ni/C). The resulting slurry was filtered and washed with de-ionized water and ethanol five times. Finally, the Pd-Ni/C catalysts were obtained by drying at 105 $^oC$ for 12 h. The theoretical Pd and Ni precursor contents of the Ni-Pd/C catalysts were targeted to 20.0 mg. For comparison, cMWCNT supported Pd without $Ni_{core}$ (Pd/C) and cMWCNT supported Ni (Ni/C) were prepared by the same method.

The preparation of an anode electrode for the electrochemical investigation was proceeded as follows: A standard glassy carbon (GC) electrode (d = 3.0 mm, A = 0.07 $cm^2$) was polished with α-$Al_2O_3$ powders. The polished GC electrode was washed using double distilled water and then dried for 10 min at room temperature before use. The Pd-Ni/C slurry was prepared by dispersing 1.0 mg catalyst into a 1.0 mL ternary mixture of de-ionized water, ethanol, and 5 wt% Nafion® (10:10:1, v/v). Afterward, the 10 μL catalyst slurry was quantitatively drop-coated onto the GC electrode surface using a micropipette and dried under a 50 W halogen lamp for 15 min. The obtained Pd-Ni/C thin film electrodes were prepared for further electrochemical characterizations.

### Physicochemical characterization of the Pd-Ni/C catalysts

The X-ray diffraction (XRD) patterns were recorded using CuKα radiation (40 kV, 40 mA) and used to characterize the elemental composition, crystal structure and particle size of the metal nanoparticles by X'Pert PRO X-ray diffractometer (PANalytical, Westborough, Massachusetts, USA). The XRD characterization was performed within the angle (2θ) range from 10° to 90°, at a scanning rate of 0.02° $s^{-1}$ and an angular resolution of 0.02° of the 2θ scan. The field-emission transmission electron microscopy (FE-TEM) and scanning transmission electron microscope (STEM) with an energy-dispersive detector (EDS) were employed to characterize the dispersion morphology, size of metal particles, crystalline nature and elemental distribution of the Pd-Ni/C catalyst using a JEM-2100F transmission electron microscope with the accelerating voltage of 200 kV (JEOL, Akishima, Tokyo, Japan). The surface morphology and elemental analysis of the Pd-Ni/C catalysts were determined using JSM-5310 scanning electron microscope and energy dispersive spectrometer (SEM-EDS) (JEOL, Akishima, Tokyo, Japan).

### Eletrochemical characterization of the Pd-Ni/C catalysts catalyzed GOR

A standard three-electrode cell, connected to an electrochemical analyzer, was used to characterize the electrocatalytic behaviors of the Pd-Ni/C catalysts. The catalyst-coated GC electrode was used as a working electrode. The reference and counter electrodes were a Hg/HgO electrode (0.1 mol $L^{-1}$ NaOH solution) and a platinum wire electrode, respectively. The electrochemical measurements were performed using a programmable potentiostat-galvanostat PGSTAT30 (Metrohm Autolab, Netherlands). The electrochemical surface area (ECSA) and the GOR eletrocatalytic activity of the Pd-Ni/C catalysts were evaluated by cyclic voltammetry (CV) at a scan

rate of 50 mV $s^{-1}$. The Tafel polarization analysis was studied using linear sweep voltammetry (LSV) at 1 mV $s^{-1}$ in order to eliminate the mass transfer effect. The chronoamperomtry (CA) measurement was performed at a constant potential of +0.1 V for 1000 s and the multi-cycle cyclic voltammetry (mCV) stability was studied using CV at 100 mV $s^{-1}$ for 500 cycles. All electrochemical measurements were performed in a deoxygenated test solution. Pd-Ni/C (1:0.06) was prepared for a further study at the different operating temperatures to obtain the activation energy value. The effects of the concentrations of glucose and NaOH were evaluated to find an optimal operating condition for attaining a higher GOR current density. The obtained currents were normalized to the geometrical area of the working GC electrode (0.07 $cm^2$).

## Results and discussion

### XRD patterns of the Pd-Ni/C catalysts

XRD was used to reveal the crystal phase and characterize their atomic structures of the Pd-Ni/C catalysts, as shown in Fig. 2A. The first diffraction peak at 25° is the graphite (0 0 2) facet of cMWCNT (JCPDS card No.: 25-0284) for all of the Pd-Ni/C catalysts. The resultant XRD patterns of Pd/C show that there are four main diffraction peaks, at 38°, 45°, 67° and 79°, which are attributed to the face-centered cubic (fcc) phase of Pd (1 1 1), (2 0 0), (2 2 0) and (3 1 1) (JCPDS card No.: 05-0681), respectively.[20] The diffraction peaks of Ni/C at 40° and 47° correspond to the face-centered cubic (fcc) phase of Ni (1 1 1) and Ni (2 0 0) (JCPDS card No.: 04-0850), respectively.[16] In addition, the peaks of Ni (1 1 1) and Ni (2 0 0) have not obviously been found on $Pd_{shell}Ni_{core}$, this is possibly because the existing Ni atom amounts are too low and $Ni_{core}$ nanoparticles are coated by $Pd_{shell}$ catalysts.

In order to determine whether Ni elements exist in the Pd-Ni/C catalysts, the atomic characterization was performed by the SEM-EDS measurement. The EDS result shows that Ni elements are composed in the Pd-Ni/C catalysts, as shown in Fig. S1. Furthermore, the average crystallize sizes of the $Pd_{shell}Ni_{core}$ nanoparticles are estimated using the diffraction peak of Pd (2 2 0) at 65° through the Debye-Scherrer equation, as written in Eq. (1).

$$d = \frac{\kappa\lambda}{FWHM \cdot \cos\theta} \qquad (1)$$

Where d is the average particle size (nm), FWHM is the full width at half-maximum of the peak expressed in radian, λ is the corresponding wavelength of the X-ray used (1.54 A°), θ is the angle of the maximum the peak patterns (rad) and K is a numerical constant of about 0.9. The estimated Pd crystallite sizes for Pd/C, Pd-Ni/C (1:0.02), Pd-Ni/C (1:0.03), Pd-Ni/C (1:0.06), Pd-Ni/C (1:0.14) and Pd-Ni/C (1:0.33) are respectively 5.7, 6.0, 6.7, 6.7, 4.9 and 5.3 nm, as shown in Table 1. The diffraction peaks of Pd (2 0 0) and Pd (2 2 0) for Pd-Ni/C (1:0.06) both shift to the higher 2θ values compared to Pd/C, as shown in Fig. 2B. This means that the insertion of Ni atom into Pd crystal lattice and Pd-Ni might form a bimetallic alloy in some degree.[16, 17] According to the HR-TEM characterization (Fig. 3), most of Pd-Ni/C bimetallic catalysts exist in core-shell structure rather than the simple alloy composite.

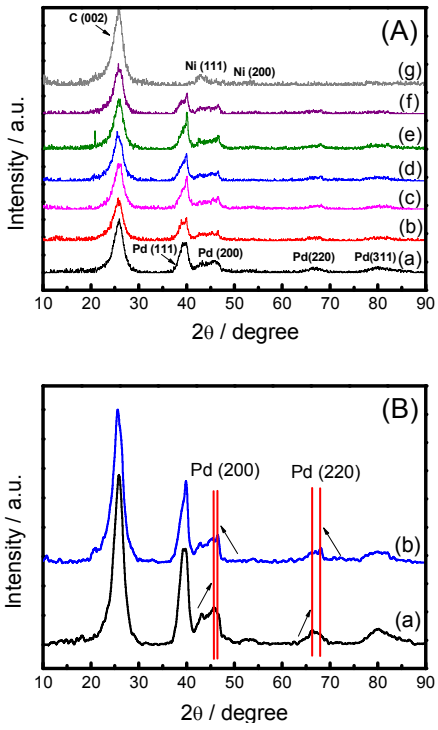


**Figure 2**. XRD patterns of (A) the Pd-Ni/C catalysts: (a) Pd/C, (b) Pd-Ni/C (1:0.02), (c) Pd-Ni/C (1:0.03), (d) Pd-Ni/C (1:0.06), (e) Pd-Ni/C (1:0.14), (f) Pd-Ni/C (1:0.33) and (g) Ni/C. The enlarged XRD patterns of (B): (a) Pd/C and (b) Pd-Ni/C (1:0.06).

The corresponding particle sizes, dispersion and surface morphology of the $Pd_{core}Ni_{shell}$ nanoparticles were characterized by TEM measurement, as shown in Fig. S2. As a result of particle size analysis in Table 1, the metal particles become smaller while Pd core metal is replaced by the certain amounts of Ni. It can be noted that Pd-Ni/C (1:0.06) exhibits the smallest particle size of 4.1 nm. In addition, $Pd_{shell}Ni_{core}$ nanocatalysts show the better metal particles dispersion on cMWCNT compared to Pd/C. This result means that $Ni_{core}$ not only increases the utilization of Pd catalyst but also improves the dispersion of metal nanoparticles.

**Table 1.** Physicochemical characterization of the Pd-Ni/C catalysts from TEM and XRD measurements.

| Catalyst | Pd/C | Pd-Ni/C (1:0.02) | Pd-Ni/C (1:0.03) | Pd-Ni/C (1:0.06) | Pd-Ni/C (1:0.14) | Pd-Ni/C (1:0.33) |
|---|---|---|---|---|---|---|
| Crystallite size/nm (XRD) | 5.7 | 6.0 | 6.7 | 6.7 | 4.9 | 5.3 |
| Particle size/nm (TEM) | 4.7±0.25 | 4.6±0.29 | 4.2±0.26 | 4.1±0.21 | 5.4±0.35 | 6.6±0.70 |

In order to identify the structure and understand the elemental distribution of the $Pd_{shell}Ni_{core}$, the nanostructure of an individual metal composite of Pd-Ni/C (1:0.06) was characterized by HR-TEM and HAADF-STEM with EDS, as shown in Fig. 3A and B, respectively. Fig. 3A shows the inter layer distances corresponding to (111) lattice plane for $Pd_{shell}$ and $Ni_{core}$ of single crystalline $Pd_{shell}Ni_{core}$ particle are 0.22 and 0.20 nm, respectively. In Fig. 3B, the EDS cross-sectional compositional line-profile proves that the synthesized Pd-Ni/C has the Ni core and the Pd outside shell.

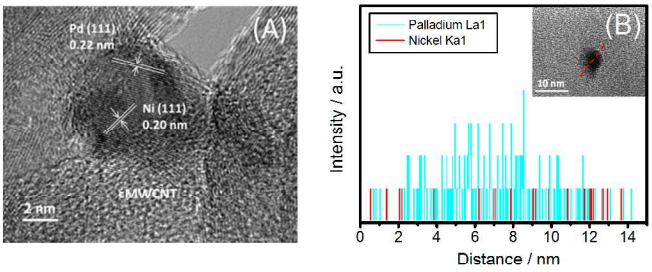


**Figure 3.** (A) HR-TEM morphological characteristic of the Pd-Ni/C catalyst; (B) Line profile of elemental compositions obtained by EDS and the insert is the corresponding HAADF-STEM image. A larger Pd-Ni nanoparticle was chosen to attain the high-quality image resolution.

### ECSA estimation and GOR characterization for the Pd-Ni/C catalysts

The voltammetric curves of the prepared catalysts, scanned in 0.5 mol $L^{-1}$ NaOH solution, are used to estimate the ECSA values, as shown in Fig. S3.[4,14] The ECSA data of the Pd-Ni catalysts are compared along with other GOR performance factors in Table 2 and have a range between 25.8 and 78.0 $m^2$ $g^{-1}$. The result indicates that Pd/C has the lowest ECSA value of 17.3 $m^2$ $g^{-1}$ and Pd-Ni/C (1:0.06) exhibits the highest ECSA value of 78.0 $m^2$ $g^{-1}$. This can prove that the core-shell structure obviously increases the electroactive surface areas of the Pd-Ni/C catalysts.

**Table 2.** Comparison between the electrocatalytic GOR properties of the Pd-Ni/C catalysts characterized by cyclic voltammograms.

| Catalyst | Onset Potential[a] (V vs. Hg/HgO) | Anodic peak ($I_f$) | | Cathodic peak ($I_b$) | | ECSA ($m^2$ $g^{-1}$) |
|---|---|---|---|---|---|---|
| | | Peak potential (V vs. Hg/HgO) | Peak current (mA $cm^{-2}$) | Peak potential (V vs. Hg/HgO) | Peak current (mA $cm^{-2}$) | |
| Pd/C | -0.53 | +0.06 | 14.2 | -0.27 | 13.2 | 17.3 |
| Pd-Ni/C (1:0.02) | -0.53 | +0.08 | 16.7 | -0.08 | 15.9 | 25.8 |
| Pd-Ni/C (1:0.03) | -0.56 | +0.01 | 18.8 | -0.26 | 17.8 | 35.4 |
| Pd-Ni/C (1:0.06) | -0.63 | +0.02 | 21.2 | -0.25 | 20.6 | 78.0 |
| Pd-Ni/C (1:0.14) | -0.56 | +0.06 | 13.8 | -0.25 | 12.5 | 70.7 |
| Pd-Ni/C (1:0.33) | -0.53 | -0.04 | 3.3 | -0.31 | 2.5 | 47.5 |

[a] Onset potential is defined as the potential at which 0.1 mA $cm^{-2}$ current density is reached.

Furthermore, Pd-Ni/C catalyzed GOR was characterized in 0.5 mol $L^{-1}$ NaOH solution containing 0.5 mol $L^{-1}$ glucose using CV measurement with a potential range of -0.8 V to +0.8 V. In Fig. 4A, the forward and backward scans of Pd/C catalyzed GOR both show a GOR peak and the corresponding peak current densities are respectively expressed as $I_f$ and $I_b$ in Table 2. In the forward scan, the GOR current density is observed at an onset potential of ca. -0.5 V for the Pd-Ni/C catalysts. It has been known that the onset of the GOR peak current density indicates the chemisorption of glucose molecules to form adsorbed intermediates and starting to release electrons. The decline of the GOR current density is observed after the peak potential due to the accumulation of the intermediates on the active site. Consequently, the coverage of Pd-Ni/C electroactive sites will inhibit the electrooxidation of glucose. The inset of Fig. 4B shows that Pd-Ni/C (1:0.06) has the highest current density of 21.2 mA $cm^2$, which is 1.5-fold higher than that for Pd/C (14.2 mA $cm^2$). This indicates that the Pd-Ni/C catalysts can enhance the GOR current densities due to its highest ECSA.

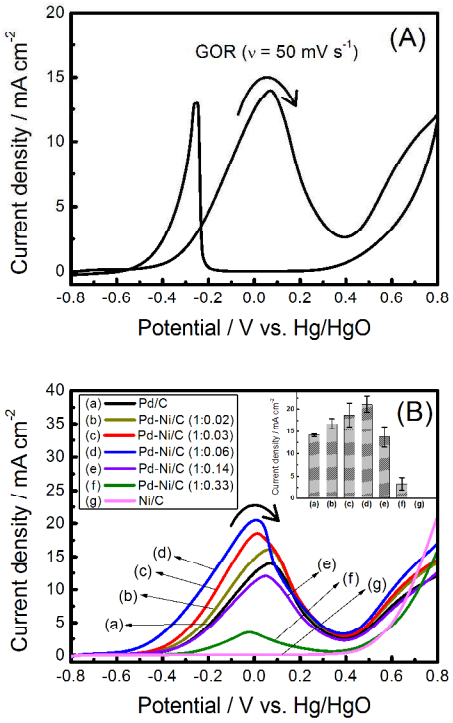


**Figure 4.** Cyclic voltammograms of (A) Pd/C and (B) the forward scan curve for Pd-Ni/C catalysts (a) Pd/C, (b) Pd-Ni/C (1:0.02), (c) Pd-Ni/C (1:0.03), (d) Pd-Ni/C (1:0.06), (e) Pd-Ni/C (1:0.14), (f) Pd-Ni/C (1:0.33) and (g) Ni/C in 0.5 mol $L^{-1}$ NaOH solution containing 0.5 mol $L^{-1}$ glucose at a scan rate of 50 mV $s^{-1}$ at room temperature.

### Kinetic property of Tafel characterization on the Pd-Ni/C catalysts

To study the kinetic property of the Pd-Ni/C catalysts, the Tafel slopes for alkaline GOR were determined by a slow-scan LSV measurement (at 1 mV $s^{-1}$) and were analyzed in Fig. 5. The rather low scan rate was taken in order to eliminate the mass transfer effect. The polarization curves depicted in Fig. 5 show two linear regions that are distinguished by an over potential ($\eta_{IR\text{-}free}$) of ca. +0.35 V.

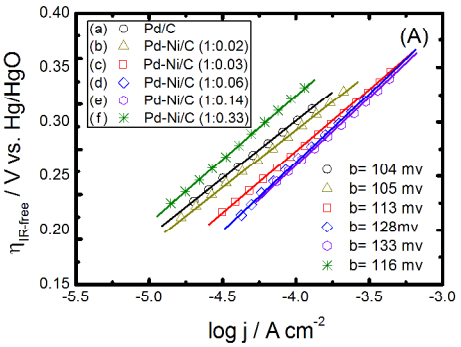

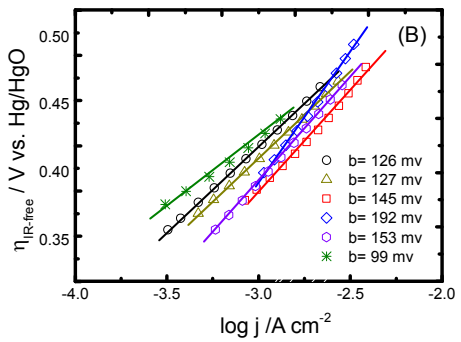


**Figure 5.** Tafel plots with linear polarization curves at (A) region I and (B) region II of the Pd-Ni/C catalysts (a) Pd/C, (b) Pd-Ni/C (1:0.02), (c) Pd-Ni/C (1:0.03), (d) Pd-Ni/C (1:0.06), (e) Pd-Ni/C (1:0.14) and (f) Pd-Ni/C (1:0.33) for GOR in 0.5 mol $L^{-1}$ NaOH solution containing 0.5 mol $L^{-1}$ glucose at a scan rate of 1 mV $s^{-1}$ at room temperature.

The Tafel plots at the lower potential (region I) are ascribed to the adsorption of hydroxyl groups and those at the higher potential (region II) are the formation of an oxide layer on the catalyst surface contributes, as shown in Fig. 5A and B, respectively.[24] The Tafel slopes for region I which were determined for Pd/C, Pd-Ni/C (1:0.02), Pd-Ni/C (1:0.03), Pd-Ni/C (1:0.06), Pd-Ni/C (1:0.14) and Pd-Ni/C (1:0.33) are 104, 105, 113, 128, 133 and 116 mV. In addition, those for the Tafel plots in region II are 126, 127, 145, 192, 153 and 99 mV, respectively. For the $Pd_{shell}Ni_{core}$ catalysts, the Tafel slopes are associated with the specific values of the properties of $Pd_{shell}$ surface by the underlying $Ni_{core}$. It can be noted that the Tafel slopes gradually change to the higher values when the core metal Pd was replaced with Ni metal. The corresponding exchange current densities were also evaluated by extrapolating the Tafel plots to the over potential equals to zero. The exchange current densities for Pd/C, Pd-Ni/C (1:0.02), Pd-Ni/C (1:0.03), Pd-Ni/C (1:0.06), Pd-Ni/C (1:0.14) and Pd-Ni/C (1:0.33) are $1.33\times10^{-4}$, $1.64\times10^{-4}$, $3.80\times10^{-4}$, $8.81\times10^{-4}$, $1.05\times10^{-3}$ and $1.47\times10^{-4}$ mA $cm^{-2}$, respectively. The result shows that Pd-Ni/C (1:0.14) performs the highest exchange current density of $1.05\times10^{-3}$ mA $cm^{-2}$, which is 7.9 times higher than that of Pd/C. Furthermore, the corresponding activation energy is estimated using the Arrhenius plot and calculated from the GOR peak current density, as shown in Fig. S4.[25] The $E_a$ values for Pd/C and Pd-Ni/C (1:0.06) are 23.1 and 16.9 kJ $mol^{-1}$, respectively, which means that $Pd_{shell}Ni_{core}$ also have the improved kinetic property on alkaline GOR.

### Poisoning rate evaluation of the Pd-Ni/C catalysts by CA measurement

To understand the catalyst stability toward GOR, the poisoning rates were studied using a chronoamperometric method. The steady-state current density at a constant exerted potential of +0.1 V is plotted against time for 1000 s at 25 °C and the results are shown in Fig. 6A. The poisoning rate (δ) is calculated by measuring the decay of the current density over a time interval at a fixed voltage of +0.1 V for 500 s and the adopted equation is defined in Eq. (2).[12,14]

$$\delta = \left(100/I_0\right)\cdot\left(dI/dt\right), t > 500\ s \qquad (2)$$

Where (dI/dt), t > 500 s is the slope of the linear current decay after 500 s and $I_0$ is the current density at the start of polarization back-extrapolated from the linear current decay. There is an initial rapid decrease in the current density with time which is observed for all catalysts.

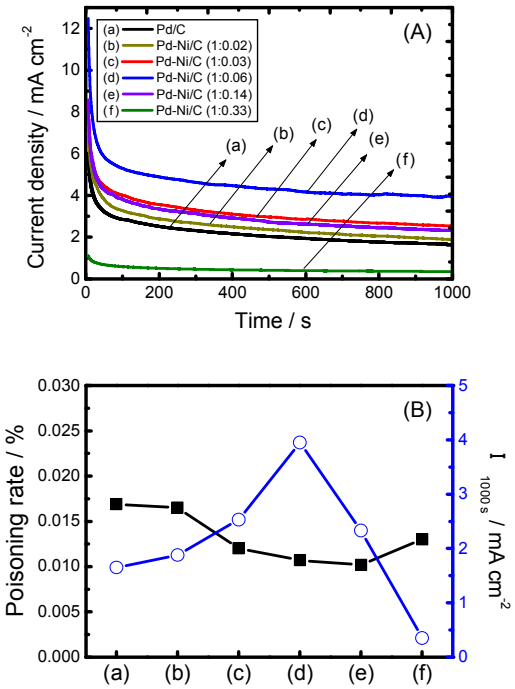


**Figure 6.** (A) Current-time curve with chronoamperometric measurements and (B) the change of the poisoning rate and the current density at 1000 s of the Pd-Ni/C catalysts for (a) Pd/C, (b) Pd-Ni/C (1:0.02), (c) Pd-Ni/C (1:0.03), (d) Pd-Ni/C (1:0.06), (e) Pd-Ni/C (1:0.14) and (f) Pd-Ni/C (1:0.33) in 0.5 mol $L^{-1}$ NaOH solution containing 0.5 mol $L^{-1}$ glucose at +0.1 V at room temperature.

This phenomenon is ascribed to the accumulation of adsorbed species on the catalyst surfaces, as shown in Fig. 6A. Afterward, the GOR current density declines slowly and reaches a steady state after 500 s. It can be found from the results that Pd-Ni/C (1:0.14) has the lowest poisoning rate $1.0\times10^{-2}$ % $s^{-1}$, as shown in Fig. 6B. The poisoning rates are also calculated as $1.7\times10^{-2}$, $1.6\times10^{-2}$, $1.2\times10^{-2}$, $1.1\times10^{-2}$ and $1.3\times10^{-2}$ % $s^{-1}$ for Pd/C, Pd-Ni/C (1:0.02), Pd-Ni/C (1:0.03), Pd-Ni/C (1:0.06) and Pd-Ni/C (1:0.33), respectively. In addition, Pd-Ni/C (1:0.06) shows the highest steady-state current density of 3.95 mA $cm^{-2}$ at 1000 s. The corresponding steady-state current densities of Pd-Ni/C catalysts are in the following order: Pd-Ni/C (1:0.06) > Pd-Ni/C (1:0.03) > Pd-Ni/C (1:0.14) > Pd-Ni/C (1:0.02) > Pd/C > Pd-Ni/C (1:0.33). Among all the prepared catalysts, Pd-Ni/C (1:0.06) has a lower poisoning rate and the highest steady-state current density according to the chronoamperometry measurement. To further study the long-term durability of Pd-Ni/C (1:0.06), a mCV study was performed in alkaline glucose medium. The retained GOR catalytic activities of Pd/C and Pd-Bi/C (1:0.06) after 500 CV cycles are 28 and 38%, respectively, as shown in Fig. S5. The results indicate that Pd-Ni/C (1:0.06) has the better poison tolerance, as well as long-term durability for alkaline GOR.

### The optimal operating condition for Pd-Ni/C (1:0.06)

To find the optimal condition of electrolyte and glucose concentrations for reaching the higher GOR current density, Pd-Ni/C

(1:0.06) catalyzes GORs with different glucose and NaOH concentrations were evaluated here.[14, 22] The range for glucose concentration is between 0 mol $L^{-1}$ and 1.0 mol $L^{-1}$ at a fixed NaOH concentration of 0.5 mol $L^{-1}$, as shown in Fig. 7A. It can be seen that the GOR current density monotonously increase to 24.1 mA $cm^{-2}$ while the glucose concentration increases to 0.5 mol $L^{-1}$, as shown in the inset of Fig. 7A. This can be explained as the dominant glucose molecules become more concentrated near the surface of Pd-Ni/C (1:0.06) by increasing glucose concentrations. However, the GOR current densities will inversely decrease when the glucose concentrations are higher than 0.5 mol $L^{-1}$. This is because too high glucose concentration (> 0.5 mol $L^{-1}$) inhibits the adsorption of hydroxyl ions on the surface of $Pd_{shell}Ni_{core}$ and GOR intermediates occupied the active sites to lower the GOR performance. Hence there is a maximum GOR current density of 24.1 mA $cm^{-2}$ at an optimal glucose concentration of 0.5 mol $L^{-1}$.

The electrocatalytic performances on Pd-Ni/C (1:0.06) with different NaOH concentrations were also evaluated at a fixed glucose concentration of 0.5 mol $L^{-1}$, as shown in Fig. 7B. The GOR current densities monotonously increase when the NaOH concentration increases from 0.25 mol $L^{-1}$ to 1.0 mol $L^{-1}$, as shown in the inset of Fig. 7B. When the NaOH concentrations are further higher than 1.0 mol $L^{-1}$, the current densities will inversely decline. It is noted that the appropriate NaOH concentration can give the faster kinetic on GOR but the too high NaOH concentration will lead to decrease the GOR current density. It can be found that there is an optimal NaOH concentration (1.0 mol $L^{-1}$) to obtain the highest Pd-Ni/C (1:0.06) catalyzes GOR current density of 34.2 mA $cm^{-2}$. Moreover, the over potential values gradually change to more negative when the NaOH concentrations increase. This phenomenon proves that hydroxyl ions effectively enhance the catalytic activities. As a result of the effects of glucose and NaOH electrolyte concentrations, the highest GOR current density of 34.2 mA $cm^{-2}$ is obtained in the 1.0 mol $L^{-1}$ NaOH solution with 0.5 mol $L^{-1}$ glucose.

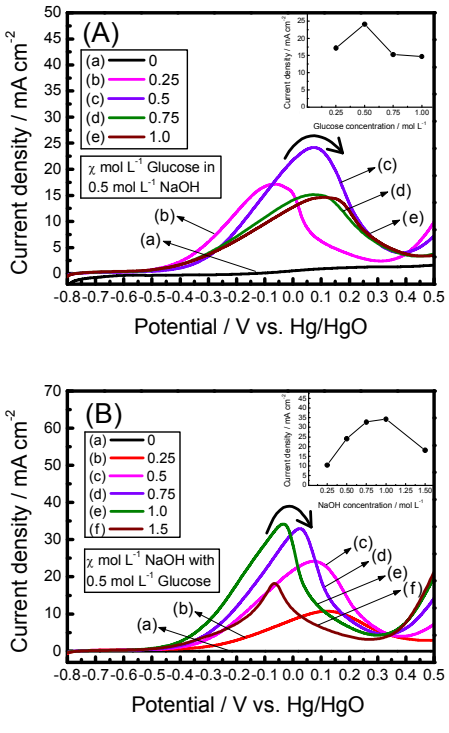


**Figure 7.** Concentration effect of Pd-Ni/C (1:0.06) at (A) different glucose concentration (0 mol $L^{-1}$ - 1 mol $L^{-1}$) in 0.5 mol $L^{-1}$ NaOH solution and (B) different NaOH concentration solution (0 mol $L^{-1}$ - 1.5 mmol $L^{-1}$) with 0.5 mol $L^{-1}$ glucose at a scan rate of 50 mV $s^{-1}$ at room temperature.

## Conclusions

Pd-Ni/C nanocatalysts with a core-shell structure have been successfully synthesized using a two-stage polyol method and are extensively studied in this work. The electrocatalytic activities and kinetics are investigated in alkaline GOR to seek an idea $Pd_{shell}Ni_{core}$ catalyst with the appropriate Pd-to-Ni ratio. Among all the prepared catalysts, Pd-Ni/C (1:0.06) has the highest ECSA (78.0 $m^2$ $g^{-1}$) and GOR current density (21.2 mA $cm^{-2}$). The possibility of the obvious improvement may be ascribed to the increase of active surface sites on the $Pd_{shell}Ni_{core}$ catalyst and the bifunctional effect. Pd-Ni/C (1:0.06) also has the lower poisoning rate ($1.1\times10^{-2}$ % $s^{-1}$), the higher long-term durability (88% activity remained) and the lower activation energy value of 16.9 kJ $mol^{-1}$ compared to Pd/C. Furthermore, the highest GOR current density of 34.2 mA $cm^{-2}$ is obtained in 1.0 mol $L^{-1}$ NaOH solution containing 0.5 mol $L^{-1}$ glucose at room temperature. To sum up, the Pd_Ni/C catalyst with a core-shell structure gives the remarkably improved GOR activity and durability, which indicates that the Pd-Ni/C is a promising non-Pt catalyst candidate in DGFC application.

## Acknowledgements

The authors gratefully acknowledge the research grant from the Ministry of Science and Technology (103-2923-E-002-008-MY3). The authors are grateful to Professor Kevin C.-W. Wu for the technical aid of the XRD analysis. Thanks to Ms. C.-Y. Chien of Ministry of Science and Technology (National Taiwan University) for the assistance in TEM experiments.

## Notes and references

*Department of Bio-Industrial Mechatronics Engineering, National Taiwan University, No. 1, Sec. 4, Roosevelt Road, Taipei 10617, Taiwan*
*Phone: ++886-2- 3366-5343 Fax: +886-2- 2362-7620.*
***Corresponding Author Email:** chenlinchi@ntu.edu.tw*

Electronic Supplementary Information (ESI) available: [details of any supplementary information available should be included here]. See DOI: 10.1039/b000000x/

[1] R.A. Bullen, T.C. Arnot, J.B. Lakeman, F.C. Walsh, 2006, **21**, 2015-2045.
[2] S. Kerzenmacher, J. Ducree, R. Zengerle, F. von Stetten, J. Power Sources, 2008, **182**, 66-75.
[3] N. Fujiwara, S. Yamazaki, Z. Siroma, T. Ioroi, H. Senoh, K. Yasuda, Electrochem. Commun., 2009, **11**, 390-392.
[4] L.L. Yan, A. Brouzgou, Y.Z. Meng, M. Xiao, P. Tsiakaras, S.Q. Song, Appl. Catal. B: Environ., 2014, **150**, 268-274.
[5] L. Li, K. Scott, E.H. Yu, J. Power Sources, 2013, **221**, 1-5.
[6] S. Kerzenmacher, J. Ducree, R. Zengerle, F. von Stetten, J. Power Sources, 2008, **182**, 1-17.
[7] D. Basu, S. Sood, S. Basu, Chem. Eng. J., 2013, **228**, 867-870.
[8] D. Basu, S. Basu, Int. J. Hydrogen Energ., 2012, **37**, 4678-4684.
[9] H.F. Cui, J.S. Ye, X. Liu, W.D. Zhang, F.S. Sheu, Nanotechnology, 2006, 17, 2334-2339.
[10] L. Hussein, Y.J. Feng, N. Alonso-Vante, G. Urban, M. Krüger, Electrochim. Acta, 2011, **56**, 7659–7665.
[11] M. Pasta, F. La Mantia, R. Ruffo, F. Peri, C. Della Pina, C.M.

Mari, J. Power Sources, 2011, **196**, 1273-1278.
[12] Sayed M. EI-Refaei, M.I. Awad, B.E. El-Anadouli, M.M. Saleh, Electrochim. Acta, 2013, **92**, 460–467.
[13] A. Brouzgou, L.L. Yan, S.Q. Song, P. Tsiakaras, Appl. Catal. B: Environ., 2014, **147**, 481-489.
[14] T.R. Ling, C.S. Li, J.J. Jow, J.F. Lee, Electrochim. Acta, 2011, **56**, 1043–1050.
[15] C.C. Chen, C.L. Lin, L.C. Chen, Electrochim. Acta, 2015, **152**, 408–416.
[16] T. Jiang, L. Yan, Y. Meng, M. Xiao, Z. Wu, P. Tsiakaras, S. Song, Appl. Catal. B: Environ., 2015, **162**, 275-281.
[17] M. Zhang, Z. Yan, J. Xie, Electrochim. Acta, 2012, **77**, 237–243.
[18] N. Kakati, J. Maiti, S.H. Lee, Y.S. Yoon, Int. J. Hydrogen Energy, 2012, **37**, 19055-19064.
[19] J.H. Jang, C. Pak, Y.U. Kwon, J. Power Sources, 2012, **201**, 179-183.
[20] M. Rashid, T.S. Jun, Y. Jung, Y.S. Kim, Sensor Actuat. B, 2015, **208**, 7-13.
[21] S.Y. Shen, T.S. Zhao, J.B. Xu, Y.S. Li, J. Power Sources, 2010, **195**, 1001-1006.
[22] C.M. Yu, M.J. Yen, L.C. Chen, Biosens. Bioelectron., 2010, **25**, 2515-2521.
[23] Z.X. Cai, C.C. Liu, G.H. Wu, X.M. Chen, X. Chen, Electrochim. Acta, 2013, **112**, 756-762.
[24] S. Alayoglu, A.U. Nilekar, M. Mavrikakis, B. Eichhorn, Nat. Mater., 2008, **7**, 333-338.
[25] Z.X. Liang, T.S. Zhao, J.B. Xu, L.D. Zhu, Electrochim. Acta, 2009, **54**, 2203-2208.
[26] J.L. Cohen, D.J. Volpe, H.D. Abruña, Phys. Chem. Chem. Phys., 2007, **9**, 49-77.